Journal of Materials Chemistry C

Evolution of short- and medium-range order in melt-quenching amorphization of Ge2Sb2Te5

Journal:	*Journal of Materials Chemistry C*
Manuscript ID	TC-ART-02-2018-000549.R3
Article Type:	Paper
Date Submitted by the Author:	10-Apr-2018

Complete List of Authors:	Qiao, Chong; Fudan University, Department of Optical Science and Engineering Shanghai, CN Guo, Y. R. ; Fudan University, Department of Optical Science and Engineering Dong, Fei; Fudan University, Department of Optical Science and Engineering Wang, Jinjin; Fudan University, Shen, Hong; Fudan University, Department of Optical Science and Engineering Wang, Songyou; Fudan University, Department of Optical Science and Engineering Xu, Ming; Huazhong University of Science and Technology, Miao, Xiangshui; Huazhong University of Science and Technology, School of Optical and Electronic Information Zheng, Y. X. ; Fudan University, Department of Optical Science and Engineering Zhang, Rongjun; Fudan University, Department of Optical Science and Engineering Chen, Liangyao; Fudan University, Wang, Cai Zhuang; Ames Laboratory-U.S. DOE, Physics and Astronomy Ho, Kai Ming; Ames Laboratory-U.S. DOE, Physics and Astronomy

Evolution of short- and medium-range order in melt-quenching amorphization of $Ge_2Sb_2Te_5$

Chong Qiao[1], Y. R. Guo [1], F. Dong[1], J. J. Wang[1], H. Shen[1], S.Y. Wang[1,2,*], Ming Xu[3,*], X. S. Miao[3], Y. X. Zheng[1], R. J. Zhang[1], L. Y. Chen[1], C. Z. Wang[4] and K. M. Ho[4]

[1]*Shanghai Ultra-Precision Optical Manufacturing Engineering Center and Department of Optical Science and Engineering, Fudan University, Shanghai, 200433, China*
[2]*Key Laboratory for Information Science of Electromagnetic Waves (MoE), Shanghai 200433, China*
[3]*Wuhan National Research Center for Optoelectronics, School of Optical & Electronic Information, Huazhong University of Science & Technology, Wuhan, 430074, China*
[4]*Ames Laboratory, U. S. Department of Energy and Department of Physics and Astronomy, Iowa State University, Ames, Iowa 50011, USA*

Corresponding Authors

***Email:** songyouwang@fudan.edu.cn **;** mxu@hust.edu.cn

Abstract

Phase-change memory takes advantage of fast phase transition between amorphous and crystalline phases of the phase-change materials (e.g., $Ge_2Sb_2Te_5$ or GST). To date, while the "SET" process (crystallization of GST glass) has been intensively studied, studies of "RESET" process (melt-quenching amorphization of GST) are still limited. In this work, we explored the structural changes of GST upon rapid cooling by *ab initio* molecular dynamics simulations and an atomistic cluster alignment (ACA) analysis. Different from other methods which only focus on the nearest bonding atoms, the ACA method can study both the short- and medium-range order clusters containing atoms beyond the first-neighbor shell and enables us to explore the changes of cluster structures in a larger scale. The results reveal that the low-coordinated octahedral clusters tend to become high-coordinated ones, and Ge-centered octahedral structures change to tetrahedrons whereas Sb-centered tetrahedrons transform to octahedral structures during the amorphization process. Interestingly, the tetrahedrons show an aggregation in liquid and supercooled liquid in

contrast to the 6-fold octahedrons which present a notable aggregation in amorphous GST. Moreover, our study showed that wrong bonds (Ge-Ge, Sb-Sb, Ge-Sb and Te-Te bonds) can promote the formation of large rings, and irreducible rings tend to separate into smaller and larger rings as the temperature is decreased. Our findings provide useful insights into the formation process and the structure of amorphous GST, which is valuable for facilitating the application of phase change materials.

Keywords: short-range structure, medium-range structure, amorphous, molecular dynamics

Introduction

Switching of materials properties can be utilized to record information in memory devices.[1-7] $Ge_2Sb_2Te_5$ (GST), as a prototypical phase-change memory material (PCM), is widely utilized in nonvolatile memory devices such as random access memory (RAM),[5-12] due to its rapid and reversible change between crystalline and amorphous phases. In past decades, the mechanism of the rapid crystallization of GST glass (i.e., the "SET" process) has been intensively studied, because the crystallization rate determines the writing speed of the data storage.[13-16] However, the "RESET" process (i.e., glass forming from the melt), which determines the power-consumption of the memory devices, appears to be less focused on.

The GST presents three structures under ambient conditions, namely, the stable hexagonal phase,[17-19] the metastable rocksalt structure[20, 21] and the amorphous state.[13, 19, 20] The GST glass is amorphized from the liquid state which has high similarity, yet with salient difference, to the amorphous structure, as advocated by Kolobov.[22] Through simulations and experiments, Schumacher et al. noticed that the viscosity of liquid GST exhibits Arrhenius behavior in the equilibrium as well as in the weakly supercooled liquid state.[23] As for the amorphous structure of GST, recent studies revealed that the local environment of Ge and Sb is usually distorted octahedrons in the first coordination shell with ABAB alternating rings (A: Ge, Sb; B: Te),[24-26] and a

global valence alternation was applied to explain such bonds in amorphous GST.[27] A further study discovered the coexistence of tetrahedral- and octahedral motifs in amorphous phase change materials, e.g., one third of Ge atoms are in the tetrahedral environment while the other atoms show a defective octahedral environment.[28] In addition, using an analytical methods based on electron charge density, the chemical-bonding network and lone pair electrons (i.e., a pair of unbonded electrons) have also been investigated to explore the structural order of amorphous GST.[29] Although these reports provide helpful information about the liquid and amorphous GST, the studies on the melt-quenching evolution of local structures are still insufficient.

In order to gain more details about the structures of liquid and amorphous GST, in this paper, we performed *ab initio* molecular dynamics simulations and analyzed the evolution of short- and medium-range order using an atomistic cluster alignment (ACA) method.[30] We show the changes of cluster structures and quantitatively determine the fraction of octahedron and tetrahedron in GST during the fast cooling process. Furthermore, we find that tetrahedrons present an aggregation behavior in liquid and supercooled states but are randomly distributed in amorphous state, whereas the octahedrons show an aggregation phenomenon only in amorphous state. Finally, ABAB and irreducible rings are also studied under amorphization process. Our results contribute to a better understanding of the glass-forming ability of GST and have implications on the design of low-power-consumption PCMs.

Methods

The *ab initio* molecular dynamics (AIMD) simulations have been performed using the Vienna ab initio simulation package (VASP) program based on the density functional theory,[31, 32] with the projector-augmented wave method[33, 34] and the Perdew-Burke-Ernzerhof generalized gradient approximation (GGA-PBE) for the exchange-correlation energy functional.[35] The initial simulation cell was a cubic supercell consisting of 42 Ge, 42 Sb and 105 Te atoms. Only Γ point was sampled

in the Brillouin zone in the AIMD simulations. The simulations were carried out at a canonical ensemble (i.e., constant number of particle, constant volume, and constant temperature (NVT) ensemble) with the periodic boundary conditions. The temperature was controlled by the Nose-Hoover thermostat.[36, 37] At the beginning of the simulation, the system was heated to 2000 K and relaxed for 30 ps in order to remove the memory effect from the initial configuration. Then, the temperature of GST was cooled down to 300 K quickly with a constant cooling rate of 0.1 K/step. The time step was set to 3 fs. Then the configurations at the temperatures of 1273, 1073, 900, 773, 623, 473 and 300 K respectively were sampled to investigate the structural properties of GST. Each sample was relaxed for 6000 MD steps at the sampled temperature to bring the system to equilibrium, and the size of simulation cell was adjusted to ensure that the internal pressure of the system was close to zero. 6000 trajectories at each sample temperature were utilized to study the structural changes in GST from liquid to amorphous state.

In this work, the ACA method,[30] which is an effective and convenient tool to investigate the short- and medium-range arrangements in liquids and glasses,[38-42] was applied to explore the structural orders of GST in different states. The short-range order (SRO) characters are classified by two types of alignment schemes. (1) The collective alignment is the first type of ACA method, e.g., a lot of clusters (center atom and its neighboring atoms) composed of the same number of atoms are selected randomly from the system, then center atoms of all the selected clusters are put in a same position and they are rigidly rotated to minimize the overall mean-square distances between different clusters. Finally, the average short-range structure is obtained with a proper isosurface value. (2) Individual cluster-template alignment is utilized to further classify the system into various types of short-range structures according to the similarity between selected cluster and given templates. In a typical run of individual cluster-template alignment, the template is fixed, and the selected single cluster is randomly rotated to minimize the mean-square distance between template and selected cluster. A direct parameter called "structure fitting score f" is straightforward to describe the structural similarity,

$$\Delta r_T^2 = \min_{C=1,\ldots,n_C} \Delta r_{C,T}^2 \quad (1)$$

$$f = \min\left(\frac{1}{n_T} \sum_{T=1}^{n_T} \Delta r_T^2 \right) \quad (2)$$

where $\Delta r_{C,T}^2$ is the distance between atom C in cluster and atom T in template. Δr_T^2 is the minimal square distance between atom T in the template and all n_C atoms in the cluster. Structure fitting score f characterizes the difference between the template (usually an undistorted octahedron or tetrahedron for GST) and the real clusters, e.g., f=0 indicates that the selected cluster has exactly the same structure to the template, and a larger f means the selected cluster has more deviation from the template. For each template, by summarizing all the clusters with the structure fitting score f less than a "cutoff", we can calculate how many clusters that resemble the template structure. The selection of the f cutoff may has some impact on the final results, e.g., larger cutoff will include more cluters with larger distortion. In our ACA analysis, we choose f = 0.2 as the cutoff so that most of relevant clusters, even with moderate distortions, are counted in. Detail procedures of both alignments can be found in Ref [30].

Results and Discussion

Figure 1(a) plots the structure factors of GST at 300 K obtained from our simulation which are in good agreement with x-ray diffraction data.[43-45] Figure 1(b) plots the total pair correlation function (PCF) of GST at different temperatures. The first peak of the PCF at 1273 K locates at the vicinity of 2.87 Å. As the temperature decreases to 300 K gradually, the first peak shifts slightly to the left but its amplitude increases remarkably, indicating that the local structure becomes more well-defined. Similar to previous studies,[23, 25, 46-48] the second and third peaks are observed below 900 K (melting point)[23] and they become more prominent with the decreasing

temperature, demonstrating that there are strong short- and medium-range[49] orders (MRO) in amorphous GST. Figure 1(c) shows the coordination numbers (CNs) of different type of atoms in GST with a cutoff distance of 3.2 Å. With the decreasing temperature, total CNs of Ge, Sb and Te atoms slightly increase to 3.88, 3.36 and 2.64 at 300 K, respectively, probably because that the liquid has low Peierls distortion and a uniform distance cutoff has excluded more atoms in liquid.[50] These values, closing to the previous report,[48] follow the "8 – N rule".[51-53] By analyzing the partial CNs, it is found that Ge and Sb atoms tend to connect with Te atoms, indicating an ABAB arrangement[17, 18] in the amorphous GST. Figure 1(d) shows the bond-angle distributions (BAD) of GST during the quenching process with a cutoff distance of 3.2 Å. In agreement with the previous studies,[24, 25, 27, 28, 45, 48, 54] the notable peaks of BADs for Ge, Sb and Te atoms locate at the vicinity of 90°, reminding us of the octahedral structures. As the temperature decreases, the peaks become stronger, indicating an increase in local octahedral order. The small peaks at the vicinity of 170° of BAD for Ge and Sb atoms reveal the distorted octahedral-like structure. As for the small shoulder at the vicinity of 60° of BAD, it suggests a triangular configuration[25] which tends to disappear eventually with the decreasing temperature.

To explore the short-range structure of GST, the ACA method,[30] which is utilized to explore the average structure in liquids and glasses by describing the local atomic packing, is applied. Collective alignment is the first part of the ACA method, here 3000 clusters, each consists of one center atom and six nearest atoms, are randomly selected from the simulation trajectories and are aligned with each other to minimize the overall mean-square distances between different clusters by rigid rotation and relative translation. By classifying the clusters according to the chemical constituent of the center atom in cluster, the common structural motifs describing the local environment of a given chemical constituent are obtained. For example, the common structures centered Ge, Sb and Te atoms at 1273, 773 and 300 K are shown in Figure 2, respectively. At 1273 K, all Ge-, Sb- and Te-centered clusters are in the disordered configurations, suggesting that there are no uniform SROs in the nearest-neighbor shells for liquid GST. In the supercooled liquid at 773 K, both the atomic-density

contours of Ge- and Sb-centered clusters present the octahedral patterns, indicating that Ge- and Sb-centered clusters begin to form octahedral configurations, but that of Te-centered cluster still presents a disorder state, illustrating Te atoms are more fragile when they connect with neighboring atoms and form local structure. When the temperature decreases to 300 K, the contours of Ge- and Sb-centered clusters become larger, demonstrating that more octahedral configurations have formed. Eventually, the contour of Te-centered cluster changes to an octahedral structure as well. We note that although all of the clusters tend to adopt the octahedral configurations at 300 K, the size and shape of atomic-density contour after alignment is different in different centered clusters, suggesting that there are some defects in the clusters such as vacancies and distortions.

Template alignment is the other part of ACA method, which can quantitatively determine the proportions of the SROs by comparing the similarity between template structure and selected clusters.[30] In previous studies,[22, 28] it is demonstrated that amorphous GST is composed of tetrahedral- and octahedral-like motifs, and amorphous and liquid GST have a similar SRO. In collective alignment part, we realize that the existence of vacancies may lead to defective octahedral-like SRO. Therefore, in our work, we build five templates (i.e., tetrahedron and 3-fold, 4-fold, 5-fold and 6-fold octahedrons) to explore the changes of tetrahedral- and octahedral-like SROs in the cooling process. In most of the previous studies in literatures,[25, 27, 48] bonding atoms (usually within a fixed cutoff distance) are mainly focused on exploring the SRO of GST. The clusters used in ACA analysis can reach neighbors beyond first neighboring shell so that it can better detect the changes of SRO or even MRO. Therefore, template alignment is an effective tool to explore the changes of short-range structures in GST during the cooling process.

Different from the analysis method with a fixed cutoff distance (as shown in Figures 1(c) and (d)), ACA method can study the local structure in a larger scale, so it provides us a new perspective on the SROs. Figure 3(a) displays the five templates (tetrahedron, 3-, 4- and 5-fold defective octahedrons and 6-fold octahedron) used to identify the types of SROs. Figures 3(b)-(e) show the fractions of total, Ge-, Sb- and

Te-centered SROs at different temperatures. Changes in the fractions of SROs are relative small from 1273 K to 900 K and 623 K to 300 K whereas they become notable from 900 K to 623 K, indicating that the structural changes primarily take place in this temperature range. In Figure 3(b), GST consists of mainly 3-, 4- and 5-fold defective octahedrons and tetrahedrons at 1273 K, with the fractions of 27.6%, 49.5%, 12.2% and 7.3%, respectively, indicating that defective octahedrons are the major theme in liquid GST and these octahedral motifs are mainly low-coordinated such as 3- and 4-fold ones. As the temperature decreases from 1273 K to 300 K, the fractions of 3- and 4-fold defective octahedrons are decreased to 13.1% and 39.7%, whereas the fractions of 5- and 6-fold octahedrons are increased to 25.1% and 13.0%, respectively, showing that the low-coordinated (3- and 4-fold) octahedrons present a tendency to become to the high-coordinated (5- and 6-fold) ones. As for tetrahedrons, the fraction reaches 8.4% at 300 K. In the whole cooling process, the fraction of total octahedral structures (sum of 3-, 4-, 5- and 6-fold octahedrons) remains ~90.5% and that of tetrahedrons stays around 8.0%, revealing that both liquid and amorphous GST are mainly composed of octahedral structures with only a small fraction of tetrahedron. Local structures other than octahedrons and tetrahedrons also exist, but they make up less than 2%.

The fractions of Ge-centered SROs with temperatures are shown in Figure 3(c). In the cooling process from 1273 K to 300 K, the fraction of 3-fold octahedron disappears gradually and that of 4-fold octahedron is decreased from 49.4% to 16.4%, while that of 5-fold octahedron is increased from 14.8% to 31.1% and that of 6-fold octahedron is increased to 26%. As a whole, the fraction of total Ge-centered octahedrons is decreased from 82.5% to 74.1%. As for the tetrahedrons, the fraction is increased from 16.7% to 25.9%, which is close to the value (27%) reported by Caravati[45] but a little smaller than his previous report with a value of 33%.[28] Then it is inferred that some Ge-centered octahedral clusters transform to Ge-centered tetrahedrons during the amorphization process.

Figure 3(d) shows the fractions of Sb-centered SROs at different temperatures. As the temperature decreases from 1273 K to 300 K, only the fraction of tetrahedron

presents a decreasing tendency in contrast to the increasing trend presented in Ge-centered SROs, the evolution trends of other four Sb-centered SROs show the similar tendencies to those of Ge-centered SROs. 3-fold octahedrons disappear gradually, the fraction of 4-fold octahedron is decreased from 52.7% to 27.3% with an abruptly decrease between 773 K and 623 K, while that of 5-fold octahedron is increased from 17.1% to 38.7% and that of 6-fold octahedron is increased to 28.9% with a notable increase between 773 K and 623 K, demonstrating that many 4-fold octahedrons change to 5- and 6-fold octahedrons in this stage. As for tetrahedrons, the fraction is decreased from 7.4% to zero, indicating that there is no Sb-centered tetrahedron in amorphous GST, in line with the previous study.[28] At the same time, the fraction of total Sb-centered octahedrons is increased from 92.1% to 97.5%, illustrating that Sb-centered tetrahedrons change to octahedral structures in the fast cooling process.

The fractions of Te-centered SROs from 1273 K to 300 K are shown in Figure 3(e). Only the fractions of 3- and 5-fold octahedrons present a similar evolution phenomenon to those of Ge- and Sb-centered configurations, the fraction of 3-fold octahedron is decreased from 35% to 22.2% while that of 5-fold octahedron is increased from 9.1% to 17.2%. Contrary to the trend in Ge- and Sb-centered SROs, the fraction of 4-fold octahedron is increased from 48.2% to 53.9%. As for tetrahedron and 6-fold octahedron, both of the fractions are close to zero in the cooling process. The fraction of total Te-centered octahedrons is of ~93% during the whole cooling process, indicating that 3-fold octahedral structures change to 4- and 5-fold octahedral structures with the decreasing temperature.

By comparing the evolution of Ge-, Sb- and Te-centered SROs shown in Figures 3(c), (d) and (e) in the fast cooling process, we find that 3- and 4-fold octahedrons in Ge- and Sb-centered clusters change to 5- and 6-fold octahedrons, and 3-fold octahedrons in Te-centered clusters change to 4- and 5-fold octahedrons. It is revealed that the low-coordinated octahedrons present a trend to change to high-coordinated octahedrons under the amorphization process. Additionally, total Ge-centered octahedrons decrease due to formation of tetrahedron, total Sb-centered octahedrons

increase due to disappearance of tetrahedron, while total Te-centered octahedrons maintain a stable proportion. The most notable feature is that substantial Ge-centered octahedral sites transform to Ge-centered tetrahedrons while Sb-centered tetrahedrons change to Sb-centered octahedral-like structures during the amorphization process.

Figure 4 displays the spatial distribution of tetrahedrons and 6-fold octahedrons (i.e., intact octahedrons without vacancies) obtained from ACA method at different temperatures. At 1273 K, most Ge-centered tetrahedrons consist of one center Ge atom and four neighboring Te atoms, presenting sp^3 hybridization. There is a large probability that Te atoms are replaced by Ge and Sb atoms, forming the so called "wrong bonds" (Ge-Ge, Sb-Sb, Ge-Sb and Te-Te bonds).[51, 55, 56] Interestingly, a few Sb-centered clusters also present the tetrahedral-like structure, in which the center Sb atoms tend to bond to Ge or Sb atoms, in line with the model proposed by Lee recently.[29] At 773 K, apart from Ge- and Sb-centered tetrahedrons, Ge- and Sb-centered 6-fold octahedrons are also obtained, they tend to bond to Te atoms with few wrong bonds. At 300 K, Sb-centered tetrahedrons disappear and only a few Ge-centered tetrahedrons survive, very similar to the results from previous study.[28] This is because the Ge-Te bonds with sp^3 hybridization is relative stable. In 6-fold octahedral structures, wrong bonds still exist, and apparently they play an important role in SRO and MRO in GST.

As the Peierls-like distortion (PLD) is one of the major structural features in phase change materials,[57-59] we also study it in the 6-fold octahedrons with different cutoff values of structure fitting scores, as shown in Figure 5. Here the PLD factor is obtained by averaging the differences of long- and short-bonds in the diagonal lines of each octahedron (e.g. a PLD factor of 0.5 Å means that the 6-fold octahedron is distorted to the extent that the "long bonds" are averagely longer than the collinear "short bonds" by 0.5 Å), and then the average PLD factor is used to characterize the distortion of each 6-fold octahedral cluster. Larger PLD factor indicates more severe distortion of central atoms in the clusters. As the cutoff value of structure fitting score increases, more 6-fold octahedral clusters are counted, and these newly included clusters resemble less to the perfect octahedral template. Interestingly, both the

distortion factors of Ge- and Sb-centered 6-fold octahedral structures concentrate at the vicinity of 0.45 Å, in line with the previous reports.[57, 58] This indicates that even though the shape of octahedral clusters may vary (characterized by different structure fitting scores), the intrinsic PLD remains at the same level and thus they may equally contribute to a similar band gap. Therefore, the PLD factor derived from ACA method can effectively reflect the distortion of local structure in amorphous GST and its electronic structure.

Traditionally, a fixed distance cutoff is used to determine the chemical environment for each atom. Very differently, the ACA method innovatively uses some standard templates to match with the clusters in atomic models. The selected clusters are allowed to bear some differences from the templates by setting a threshold of the structure fitting score. The selection of this threshold cutoff is very important, yet quite artificial. Despite of this drawback, ACA method is still an effective and innovative tool to analyze the structure of materials, particularly the liquid and amorphous systems.

To explore the evolution of medium-range order in GST upon quenching, Figures 6(a)-(c) show the connectivity of the center atoms of tetrahedrons and 6-fold octahedrons, with a cutoff distance of 5.2 Å which is at the vicinity of second valley of total pair correlation function. Figures 6(d)-(f) present the relationship of clusters corresponding to Figures 6(a)-(c), respectively. At 1273 K, there is no 6-fold octahedron, only tetrahedral clusters are observed in the simulation cell and most of them connect with each other to form a longer chain, indicating an obvious aggregation phenomenon, as seen in Figure 6(a). The tetrahedrons are connected by two ways: sharing a vertex or an edge (two vertices), and a larger MRO structure is formed by random combination of these two connecting ways, as shown in Figure 6(d). At 773 K, although the positions of tetrahedrons are different from the case at 1273 K, the clusters are still aggregated, and a few of 6-fold octahedrons are formed around the tetrahedral clusters, as seen in Figure 6(b). Among the MRO structures, tetrahedrons are connected by sharing a vertex, center atom or an edge, octahedrons are connected by sharing a vertex or an edge, and tetrahedrons and octahedrons are

connected by sharing central atom, a vertex or an edge, as shown in Figure 6(e). When the temperature decreases to 300 K, many more 6-fold octahedrons emerge and their size is still growing. The left-over tetrahedrons tend to connect with the larger clusters in a random distribution, as displayed in Figure 6(c). Further analysis of the relationship of tetrahedrons and 6-fold octahedrons at 300 K demonstrates: (1) tetrahedrons connect with each other only by vertices, (2) octahedrons connect with other octahedrons by sharing a vertex, an edge or a surface (three vertices), and (3) tetrahedrons connect with octahedrons by sharing a vertex, an edge or center atom, as shown in Figure 6(f). Same to the previous simulations,[25, 28, 45] the element aggregation is not observed, it is probably due to the limitation of supercell and simulation time. To summarize, we observe a large aggregation of tetrahedrons in the high temperature liquid (1273 K) and supercooled liquid (773 K) by sharing the vertex, edge or center atom, but these tetrahedrons are sparsely distributed in the amorphous state. In contrast, the number of 6-fold octahedrons grows fast upon cooling and they tend to connect with each other to complete the nucleation process.

To further explore the MRO structure in GST upon quenching, ring statistics are analyzed using a cutoff distance of 3.2 Å. Figure 7(a) shows the evolution of ABAB ring with temperature, where 4- and 6-membered rings are found to be dominated, suggesting that heteropolar bonds tend to form the specific short-range structure, similar to the previous report.[25] To investigate the effect of wrong bonds on the MRO in the disorder GST, irreducible rings at 1273 K, 773 K and 300 K are also studied using the ring statistics analysis code,[60] as the results are shown in Figures 7(b), (c) and (d), respectively. It can be seen that rings vary from 3-membered ring to 20-membered ring regardless of temperature, indicating the existence of short- and medium-range orders. Compare the irreducible rings to ABAB rings, apart from the short rings, many large rings (such as 9- to 20-membered rings) are also observed, suggesting that homopolar bonds play an inevitable role in MRO. At 1273 K, rings from 3-membered to 5-membered are in a large weight while the fractions of rings from 6- to 20-membered are relative small, as seen in Figure 7(b). When the temperature decreases to 773 K, the number of 3-membered rings decreases while that

of 6-membered rings increases notably. At this temperature, the fractions of 4-, 5- and 6-membered rings are the largest ones while that of 7- to 20-membered rings are very small, as shown in Figure 7(c). As the temperature decreases to 300 K, 3-membered rings almost disappear, while 4- to 6-membered rings possess an even larger weight. More interestingly, there is a small spike for the 15- to 17-membered rings, as shown in Figure 7(d). A similar phenomenon is also observed in a previous literature,[61] and this is probably due to the presence of nanocavities.[24, 62] Hence, the irreducible rings present two opposite trends under amorphization process, i.e., to become smaller rings or to change into larger ones. Additionally, it is noticed that 5-membered rings always have a large weight in the cooling process, indicating that wrong bonds also play an importance role in SROs.[25, 63]

Mean square displacement (MSD) is usually utilized to characterize atomic mobility. The MSD as a function of time is defined as follows:

$$\left\langle R_{\alpha}^{2}(t)\right\rangle = \frac{1}{N_{\alpha}}\left\langle \sum_{i=1}^{N_{\alpha}} \left| R_{i\alpha}(t+\tau) - R_{i\alpha}(\tau)\right|^{2} \right\rangle \tag{3}$$

where N_{α} is the number of α atoms, $R_{i\alpha}$ are the coordinates of atom i, and τ is the arbitrary origin of time. The MSD of total, Ge, Sb and Te atoms at different temperatures are shown in Figure 8, and all of them exhibit a nearly linear behavior in the liquid and supercooled liquid states. As the temperature decreases, the slope of MSD decreases, indicating that atomic mobility is reduced in cooling process. By comparing the MSD of Ge, Sb and Te atoms, we find that Ge atom moves fastest in liquid (above 900 K) and supercooled liquid (from 623 K to 900 K) GST, and Sb is the slowest in liquid whereas Te becomes the slowest in supercooled liquid. The diffusion coefficients are computed by the Einstein formula as follows:

$$D = \frac{1}{6}\frac{\partial}{\partial t}\lim_{t\to\infty}\left\langle R_{\alpha}^{2}(t)\right\rangle \tag{4}$$

Furthermore, diffusion coefficients also follow the Arrhenius equation:

$$D = D_{0}\exp\left(-\frac{E_{\alpha}}{k_{B}T}\right) \tag{5}$$

where D_0 is denoted as the pre-exponential factor, E_{α} is the activation energy, and k_B is

the Boltzmann constant. The relation between lnD and *1/T* is shown in Figure 9. lnD decreases with *1/T*, implying that calculated diffusion coefficient decreases with the decreasing temperature. Using the linear fitting, we obtain the pre-exponential factors and activation energies of liquid GST, respectively. The calculated pre-exponential factor and activation energy are 1.42×10^{-7} m^2/s and 0.33 eV between 1273 K and 523 K, respectively. As the temperature decreases continuously, the calculated pre-exponential factor and activation energy become 0.009×10^{-7} m^2/s and 0.08 eV, respectively, indicating the liquid turns into glass eventually.

Conclusions

In conclusion, by using first-principles calculations with the ACA analysis method, we have investigated changes of short- and medium-range structures in phase change material GST upon rapid cooling. Different from previous studies, the clusters selected for ACA analysis go beyond the first neighboring shell atoms, so that the SRO in GST can be better characterized. As the temperature decreases, we find that the low-coordinated octahedrons tend to become the high-coordinated ones upon cooling. It is also found that Ge-centered octahedral structures change to tetrahedron while Sb-centered tetrahedrons transfer to octahedral structures in the formation process of amorphous GST, and Ge-centered tetrahedrons in amorphous GST possess a fraction of 25.9% in Ge-centered configurations. Furthermore, we find that tetrahedrons show an aggregation in liquid and supercooled liquid but exhibit a random distribution in amorphous. By contrast, 6-fold octahedrons show a random distribution in supercooled liquid but an obvious aggregation in amorphous state. Specifically, tetrahedrons connect with each other directly in many ways to form a larger cluster in both liquid and supercooled liquid. While in the amorphous state, 6-fold octahedrons are connected with each other and also connected with tetrahedrons. Finally, the ABAB and irreducible rings are investigated in the fast cooling process, we realize that wrong bonds can promote the formation of large rings, and irreducible rings tend to decomposed into both smaller and larger rings as the

temperature is decreased. Our study can promote the knowledge of the formation process and structure of amorphous GST, and the analysis method can be applied to more phase change materials.

Acknowledgments

Work at Fudan University was supported by the NSF of China (Grant No. 11374055 and 61427815) and the Fudan High-end computing center. M.X. acknowledges National Key R&D Plan of China (Grant No. 2017YFB0701700 "Materials Genome Engineering"). Work at Ames Laboratory was supported by the US Department of Energy, Basic Energy Sciences, and Division of Materials Science and Engineering, including a grant of computer time at the National Energy Research Scientific Computing Centre (NERSC) in Berkeley, CA under. Ames Laboratory is operated for the U.S. DOE by Iowa State University under contract # DE-AC02-07CH11358.

References

1. H. Nili, S. Walia, S. Balendhran, D. B. Strukov, M. Bhaskaran and S. Sriram, *Adv. Funct. Mater.*, 2014, **24**, 6741-6750.
2. H. Nili, S. Walia, A. E. Kandjani, R. Ramanathan, P. Gutruf, T. Ahmed, S. Balendhran, V. Bansal, D. B. Strukov, O. Kavehei, M. Bhaskaran and S. Sriram, *Adv. Funct. Mater.*, 2015, **25**, 3172-3182.
3. H. Nili, T. Ahmed, S. Walia, R. Ramanathan, A. E. Kandjani, S. Rubanov, J. Kim, O. Kavehei, V. Bansal, M. Bhaskaran and S. Sriram, *Nanotechnology*, 2016, **27**, 505210.
4. T. Ahmed, S. Walia, J. Kim, H. Nili, R. Ramanathan, E. L. H. Mayes, D. W. M. Lau, O. Kavehei, V. Bansal, M. Bhaskaran and S. Sriram, *Nanoscale*, 2017, **9**, 14690-14702.
5. S. R. Ovshinsky, *Phys. Rev. Lett.*, 1968, **21**, 1450-1453.
6. J. Feinleib, J. Deneufville, S. C. Moss and S. R. Ovshinsky, *Appl. Phys. Lett.*, 1971, **18**, 254-257.
7. A. Pirovano, A. L. Lacaita, A. Benvenuti, F. Pellizzer and R. Bez, *Ieee T. Electron Dev.*, 2004, **51**, 452-459.
8. M. H. R. Lankhorst, B. Ketelaars and R. A. M. Wolters, *Nat. Mater.*, 2005, **4**, 347-352.
9. M. Wuttig and N. Yamada, *Nat. Mater.*, 2007, **6**, 824-832.
10. S. Raoux, G. W. Burr, M. J. Breitwisch, C. T. Rettner, Y. C. Chen, R. M. Shelby, M. Salinga, D. Krebs, S. H. Chen, H. L. Lung and C. H. Lam, *Ibm J. Res. Dev.*, 2008, **52**, 465-479.
11. G. W. Burr, M. J. Breitwisch, M. Franceschini, D. Garetto, K. Gopalakrishnan, B. Jackson, B. Kurdi, C. Lam, L. A. Lastras, A. Padilla, B. Rajendran, S. Raoux and R. S. Shenoy, *J. Vac. Sci.*

Technol. B, 2010, **28**, 223-262.

12. S. Raoux, W. Welnic and D. Ielmini, *Chem. Rev.*, 2010, **110**, 240-267.
13. A. V. Kolobov, P. Fons, A. I. Frenkel, A. L. Ankudinov, J. Tominaga and T. Uruga, *Nat. Mater.*, 2004, **3**, 703-708.
14. D. Loke, T. H. Lee, W. J. Wang, L. P. Shi, R. Zhao, Y. C. Yeo, T. C. Chong and S. R. Elliott, *Science*, 2012, **336**, 1566-1569.
15. J. Orava, A. L. Greer, B. Gholipour, D. W. Hewak and C. E. Smith, *Nat. Mater.*, 2012, **11**, 279-283.
16. F. Rao, K. Ding, Y. Zhou, Y. Zheng, M. Xia, S. Lv, Z. Song, S. Feng, I. Ronneberger, R. Mazzarello, W. Zhang and E. Ma, *Science* 2017, **358**, 1423-1426.
17. B. J. Kooi and J. T. M. De Hosson, *J. Appl. Phys.*, 2002, **92**, 3584-3590.
18. Z. M. Sun, J. Zhou and R. Ahuja, *Phys. Rev. Lett.*, 2006, **96**, 055507.
19. J. L. F. Da Silva, A. Walsh and H. Lee, *Phys. Rev. B*, 2008, **78**, 224111.
20. N. Yamada and T. Matsunaga, *J. Appl. Phys.*, 2000, **88**, 7020-7028.
21. X. Q. Liu, X. B. Li, L. Zhang, Y. Q. Cheng, Z. G. Yan, M. Xu, X. D. Han, S. B. Zhang, Z. Zhang and E. Ma, *Phys. Rev. Lett.*, 2011, **106**, 025501.
22. A. V. Kolobov, P. Fons, M. Krbal, R. E. Simpson, S. Hosokawa, T. Uruga, H. Tanida and J. Tominaga, *Appl. Phys. Lett.*, 2009, **95**, 241902.
23. M. Schumacher, H. Weber, P. Jovari, Y. Tsuchiya, T. G. A. Youngs, I. Kaban and R. Mazzarello, *Sci. Rep.*, 2016, **6**, 27434.
24. J. Akola and R. O. Jones, *Phys. Rev. B*, 2007, **76**, 235201.
25. J. Akola and R. O. Jones, *J. Phys.: Condens. Matter*, 2008, **20**, 465103.
26. N.-K. Chen, X.-B. Li, X.-P. Wang, W. Q. Tian, S. Zhang and H.-B. Sun, *Acta Mater.*, 2018, **143**, 102-106.
27. M. Xu, Y. Q. Cheng, H. W. Sheng and E. Ma, *Phys. Rev. Lett.*, 2009, **103**, 195502.
28. S. Caravati, M. Bernasconi, T. D. K hne, M. Krack and M. Parrinello, *Appl. Phys. Lett.*, 2007, **91**, 171906.
29. T. H. Lee and S. R. Elliott, *Adv. Mater.*, 2017, **29**, 1700814.
30. X. W. Fang, C. Z. Wang, Y. X. Yao, Z. J. Ding and K. M. Ho, *Phys. Rev. B*, 2010, **82**, 184204
31. G. Kresse and J. Hafner, *Phys. Rev. B*, 1993, **47**, 558-561.
32. G. Kresse and J. Furthmuller, *Comp. Mater. Sci.*, 1996, **6**, 15-50.
33. P. E. Blochl, *Phys. Rev. B*, 1994, **50**, 17953-17979.
34. G. Kresse and D. Joubert, *Phys. Rev. B*, 1999, **59**, 1758-1775.
35. J. P. Perdew, K. Burke and M. Ernzerhof, *Phys. Rev. Lett.*, 1996, **77**, 3865-3868.
36. W. G. Hoover, *Phys. Rev. A*, 1985, **31**, 1695-1697.
37. S. Nose, *J. Chem. Phys.*, 1984, **81**, 511-519.
38. L. H. Xiong, K. Chen, F. S. Ke, H. B. Lou, G. Q. Yue, B. Shen, F. Dong, S. Y. Wang, L. Y. Chen, C. Z. Wang, K. M. Ho, X. D. Wang, L. H. Lai, H. L. Xie, T. Q. Xiao and J. Z. Jiang, *Acta Mater.*, 2015, **92**, 109-116.
39. M. Wu, J. S. Tse, S. Y. Wang, C. Z. Wang and J. Z. Jiang, *Nat. Commun.*, 2015, **6**, 6493.
40. Y. Zhang, C. Z. Wang, M. I. Mendelev, F. Zhang, M. J. Kramer and K. M. Ho, *Phys. Rev. B*, 2015, **91**, 180201.
41. L. H. Xiong, X. D. Wang, Q. Yu, H. Zhang, F. Zhang, Y. Sun, Q. P. Cao, H. L. Xie, T. Q. Xiao, D. X. Zhang, C. Z. Wang, K. M. Ho, Y. Ren and J. Z. Jiang, *Acta Mater.*, 2017, **128**, 304-312.

42. X.-D. Wang and J.-Z. Jiang, *Adv. Mater.*, 2017, **29**, 1703136.
43. S. Kohara, K. Kato, S. Kimura, H. Tanaka, T. Usuki, K. Suzuya, H. Tanaka, Y. Moritomo, T. Matsunaga, N. Yamada, Y. Tanaka, H. Suematsu and M. Takata, *Appl. Phys. Lett.*, 2006, **89**, 201910.
44. W. Zhang, V. L. Deringer, R. Dronskowski, R. Mazzarello, E. Ma and M. Wuttig, *Mrs Bull.*, 2015, **40**, 856-869.
45. S. Caravati, M. Bernasconi, T. D. Kuehne, M. Krack and M. Parrinello, *J. Phys.: Condens. Matter*, 2009, **21**, 255501.
46. C. Steimer, V. Coulet, W. Welnic, H. Dieker, R. Detemple, C. Bichara, B. Beuneu, J.-P. Gaspard and M. Wuttig, *Adv. Mater.*, 2008, **20**, 4535-4540.
47. J. Hegedus and S. R. Elliott, *Nat. Mater.*, 2008, **7**, 399-405.
48. E. Cho, J. Im, C. Park, W. J. Son, D. H. Kim, H. Horii, J. Ihm and S. Han, *J. Phys.: Condens. Matter*, 2010, **22**, 205504.
49. S. R. Elliott, *Nature*, 1991, **354**, 445-452.
50. M. Delheusy, J. Y. Raty, R. Detemple, W. Welnic, M. Wuttig and J. P. Gaspard, *Physica B*, 2004, **350**, e1055–e1057.
51. P. Jovari, I. Kaban, J. Steiner, B. Beuneu, A. Schops and A. Webb, *J. Phys.: Condens. Matter*, 2007, **19**, 335212.
52. P. Jovari, I. Kaban, J. Steiner, B. Beuneu, A. Schoeps and M. A. Webb, *Phys. Rev. B*, 2008, **77**, 035202.
53. N. F. Mott, *Adv. Phys.*, 1967, **16**, 49.
54. F.-C. Pang, D. Wang, N.-K. Chen, S.-Y. Xie, X. Meng, C.-S. Huo, H. Yang, X.-P. Su, W.-Q. Wang and H.-L. Tu, *Comp. Mater. Sci.*, 2012, **61**, 287-290.
55. T. H. Lee and S. R. Elliott, *Phys. Rev. Lett.*, 2011, **107**, 145702.
56. J. Kalikka, J. Akola, J. Larrucea and R. O. Jones, *Phys. Rev. B*, 2012, **86**, 144113.
57. M. Xu, Z. Yu, L. Wang, R. Mazzarello and M. Wuttig, *Adv. Electron. Mater.*, 2015, **1**, 1500240.
58. J. Y. Raty, W. Zhang, J. Luckas, C. Chen, R. Mazzarello, C. Bichara and M. Wuttig, *Nat. Commun.*, 2015, **6**, 7467.
59. J. Y. Raty, V. Godlevsky, P. Ghosez, C. Bichara, J. P. Gaspard and J. R. Chelikowsky, *Phys. Rev. Lett.*, 2000, **85**, 1950-1953.
60. S. Le Roux and P. Jund, *Comp. Mater. Sci.*, 2010, **49**, 70-83.
61. S. Gabardi, S. Caravati, M. Bernasconi and M. Parrinello, *J. Phys.: Condens. Matter*, 2012, **24**, 385803.
62. S. Caravati, M. Bernasconi and M. Parrinello, *Phys. Rev. B*, 2010, **81**, 014201.
63. K. Ohara, L. Temleitner, K. Sugimoto, S. Kohara, T. Matsunaga, L. Pusztai, M. Itou, H. Ohsumi, R. Kojima, N. Yamada, T. Usuki, A. Fujiwara and M. Takata, *Adv. Funct. Mater.*, 2012, **22**, 2251-2257.

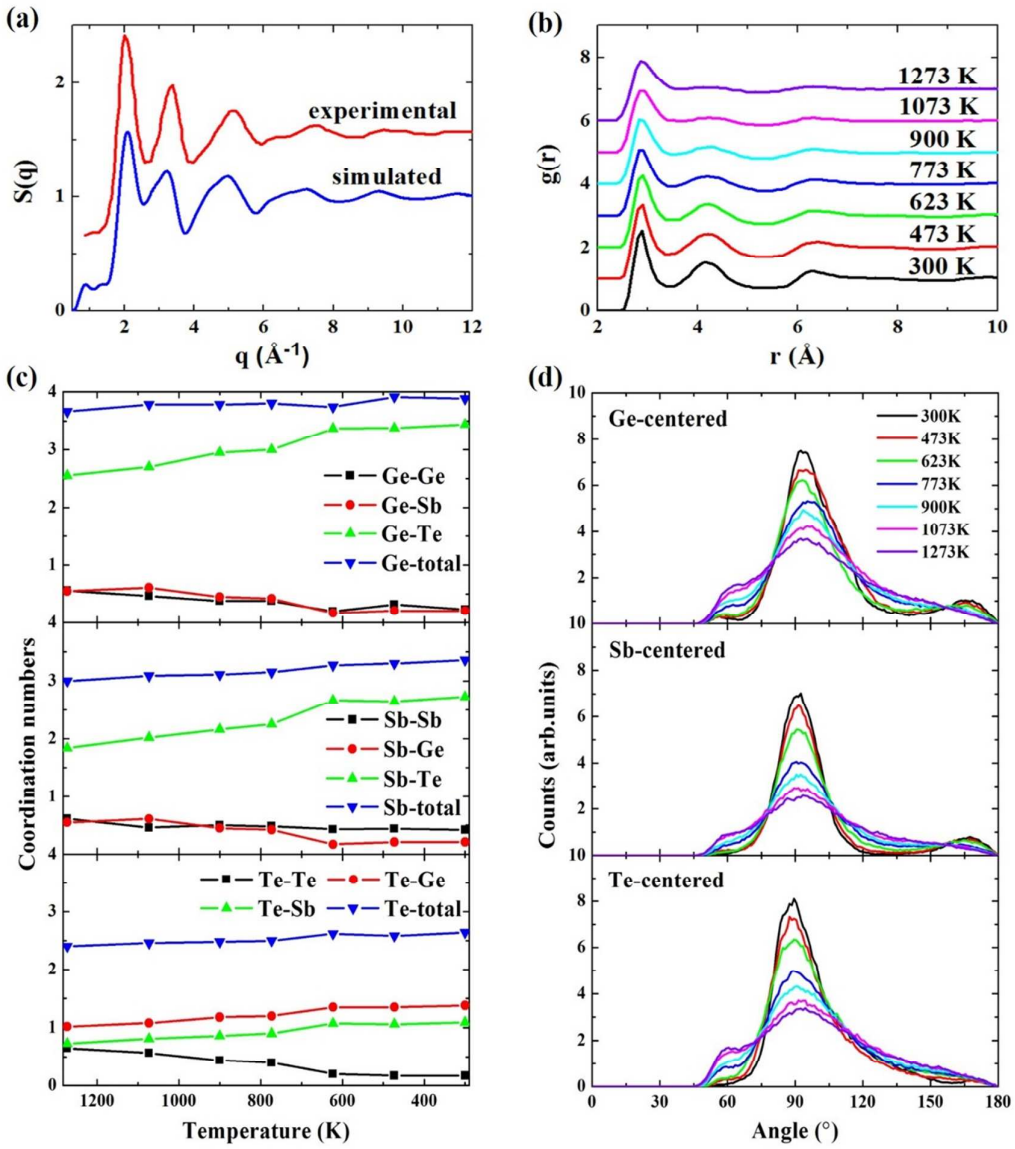

Figure 1. (a) The experimental and calculated structure factors at 300 K. (b) Total PCFs, (c) CNs and (d) BADs of GST when it is quenched from liquid to glass.

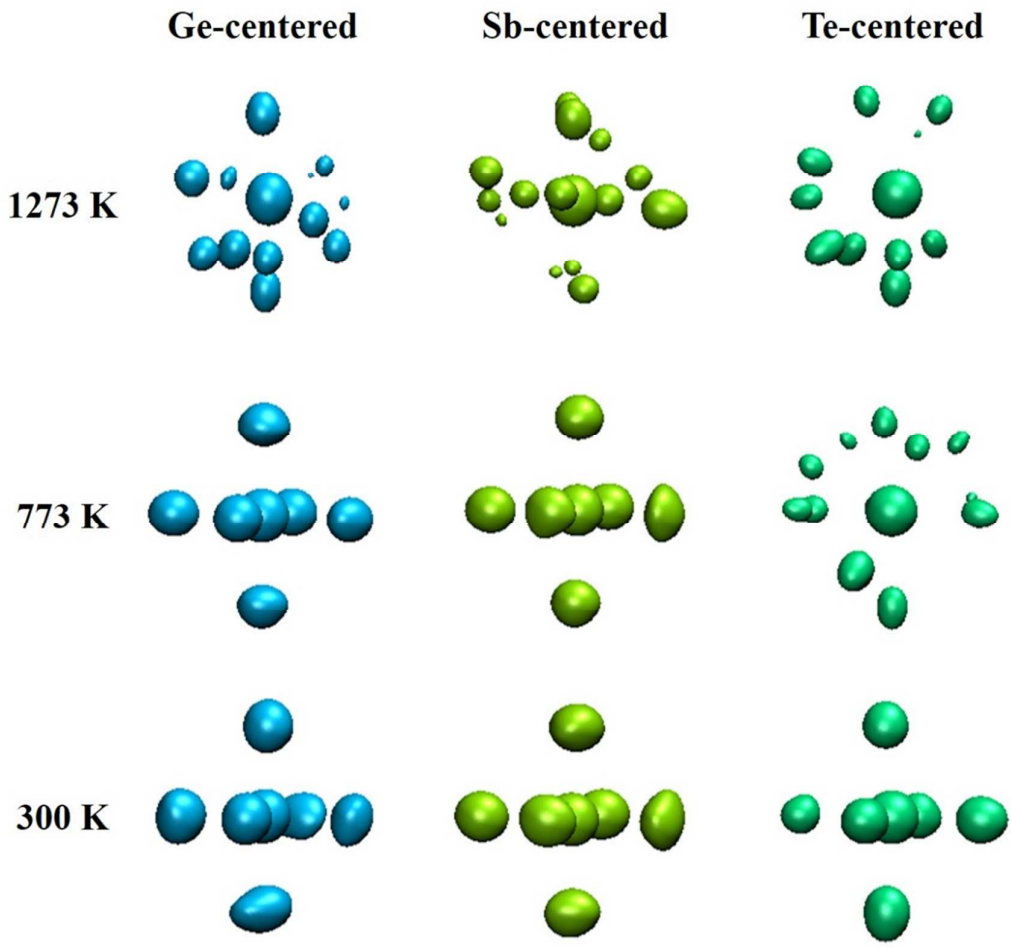

Figure 2. Atomic-density contour plot of GST from the cluster alignment method at selected three temperatures of 1273, 773 and 300 K, respectively, with the iso-surface value of 0.25 $Å^{-3}$. Cyan, yellow and green contour plots represent the SROs of Ge-, Sb- and Te-centered clusters.

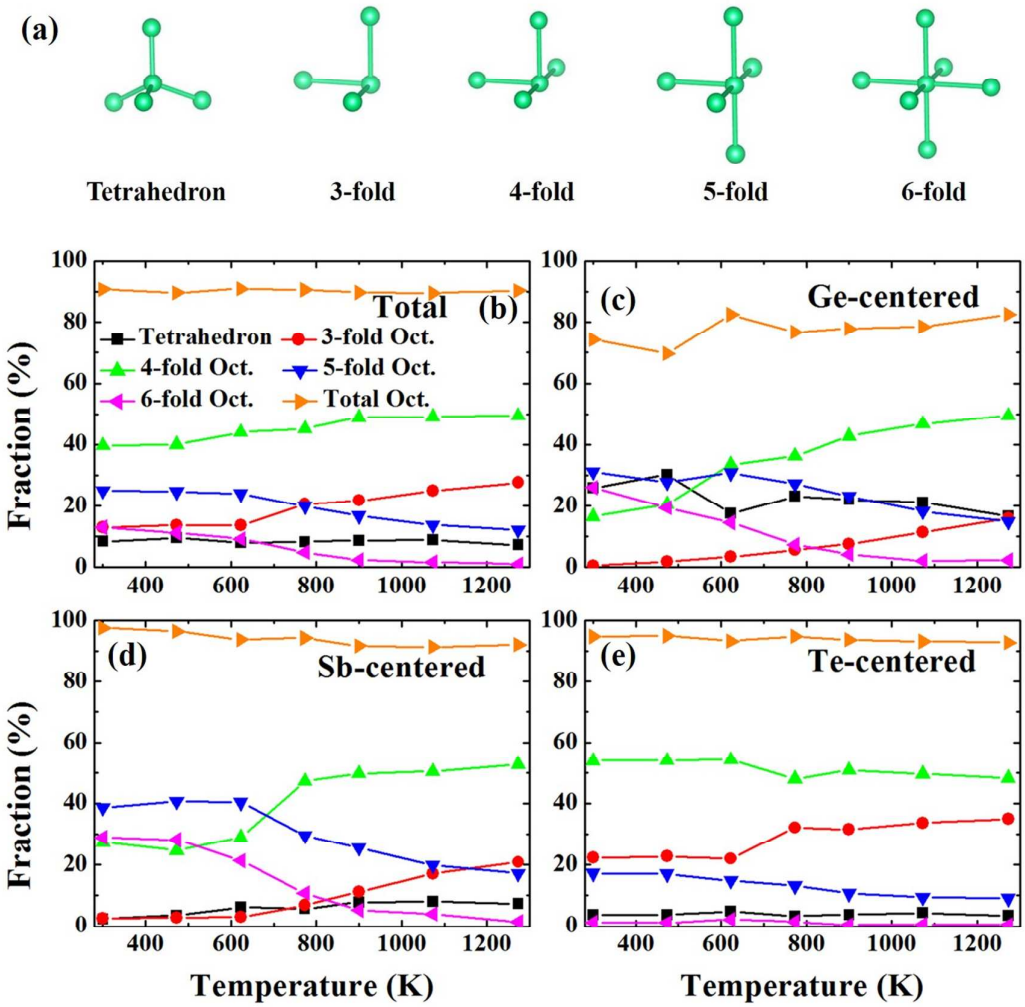

Figure 3. (a) Five templates: tetrahedron, 3-, 4- and 5-fold octahedrons (defective octahedrons) and 6-fold octahedron. (b) - (e) the fractions of the five templates at different temperatures.

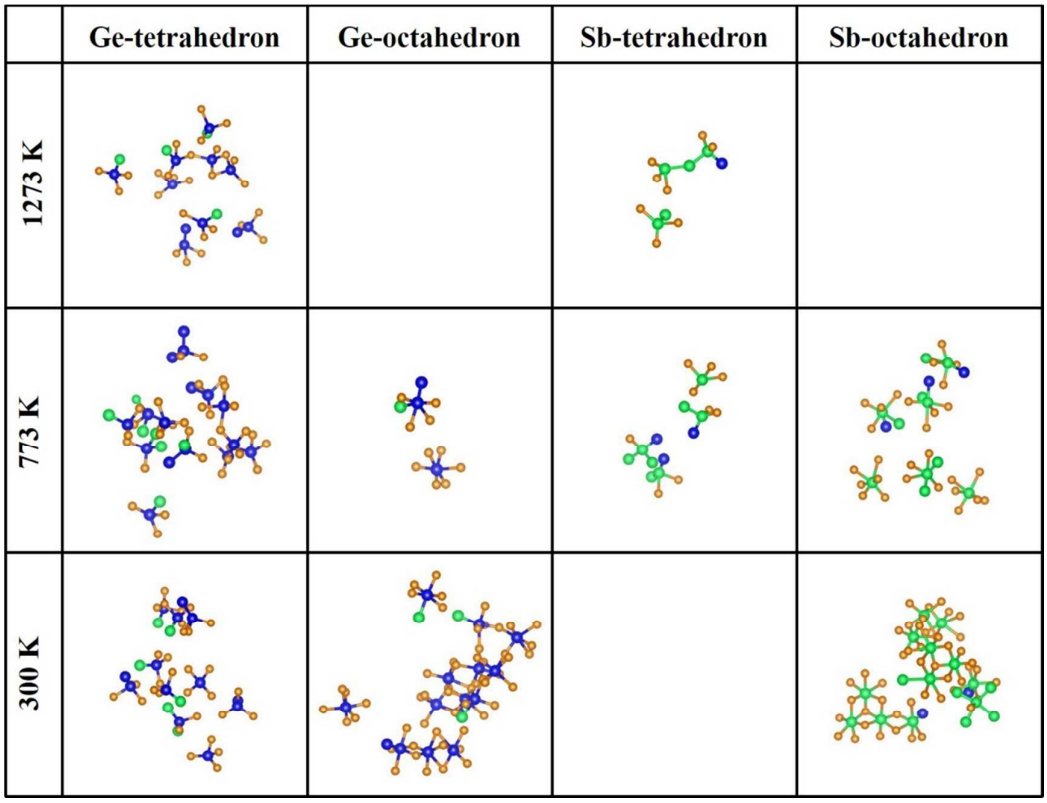

Figure 4. Distributions of tetrahedron and 6-fold octahedron centered Ge and Sb atoms at different temperatures. Blue, green and orange spheres denote Ge, Sb and Te atoms.

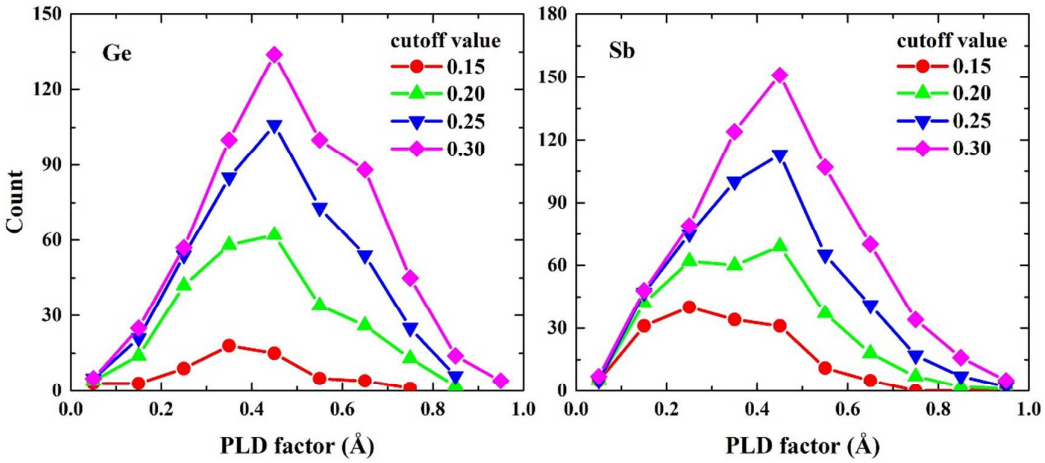

Figure 5. The distribution of Ge- and Sb-centered 6-fold octahedrons at different PLD factors when we choose different cutoff values of structure fitting scores at 300 K.

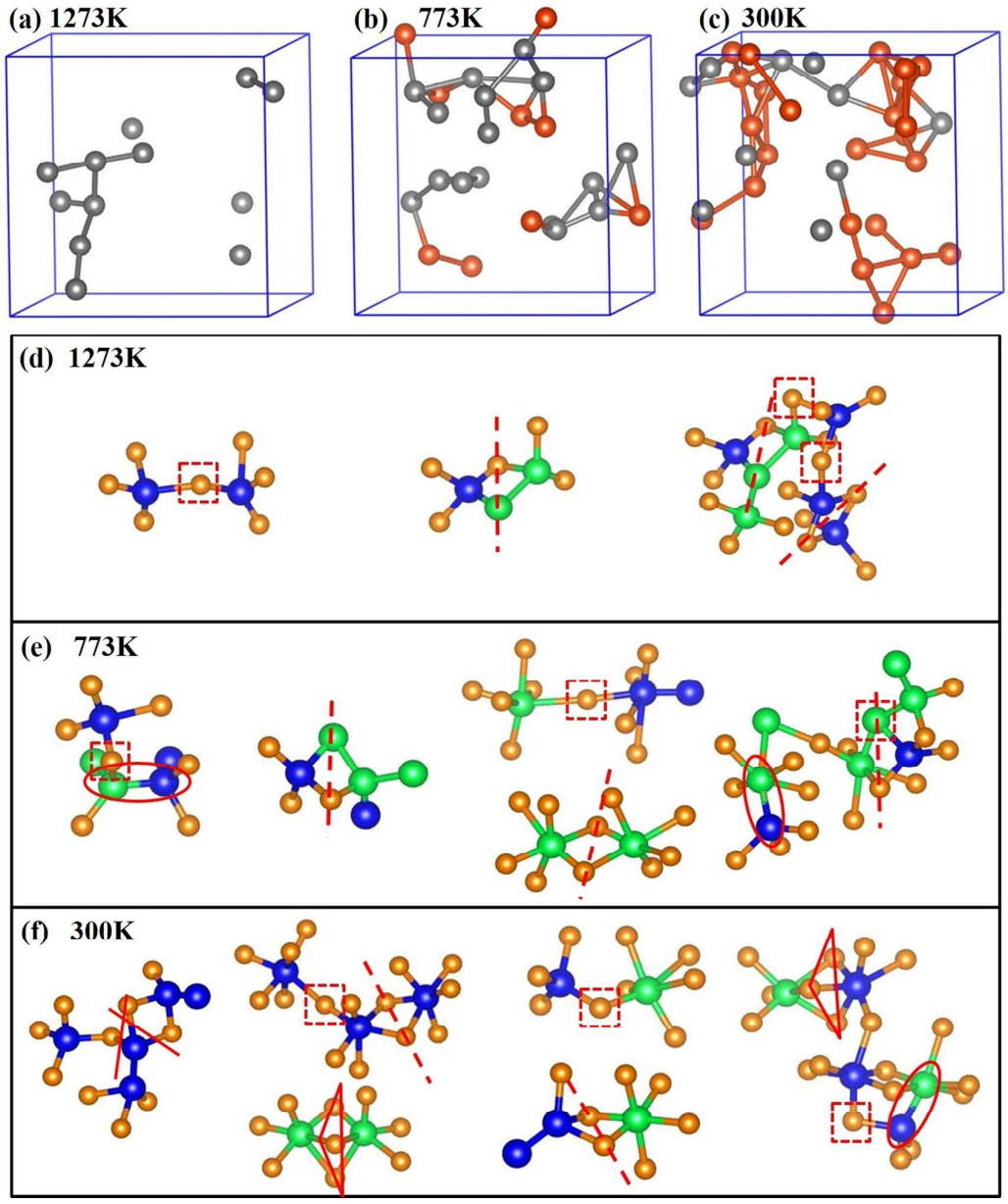

Figure 6. Distribution and connectivity of tetrahedrons and 6-fold octahedrons. Only the central atom of each cluster is depicted. Dark and red spheres denote the center atoms forming tetrahedrons and 6-fold octahedrons at (a) 1273 K, (b) 773 K and (c) 300 K, respectively. (d), (e) and (f) correspond to (a), (b) and (c), presenting the connectivity of clusters. A square, a dashed line and a triangle represent that clusters connect by sharing one, two and three vertices, respectively. Ellipse represents the central atoms of two clusters connect with each other. Solid red line denotes clusters connect by the bonding of vertices.

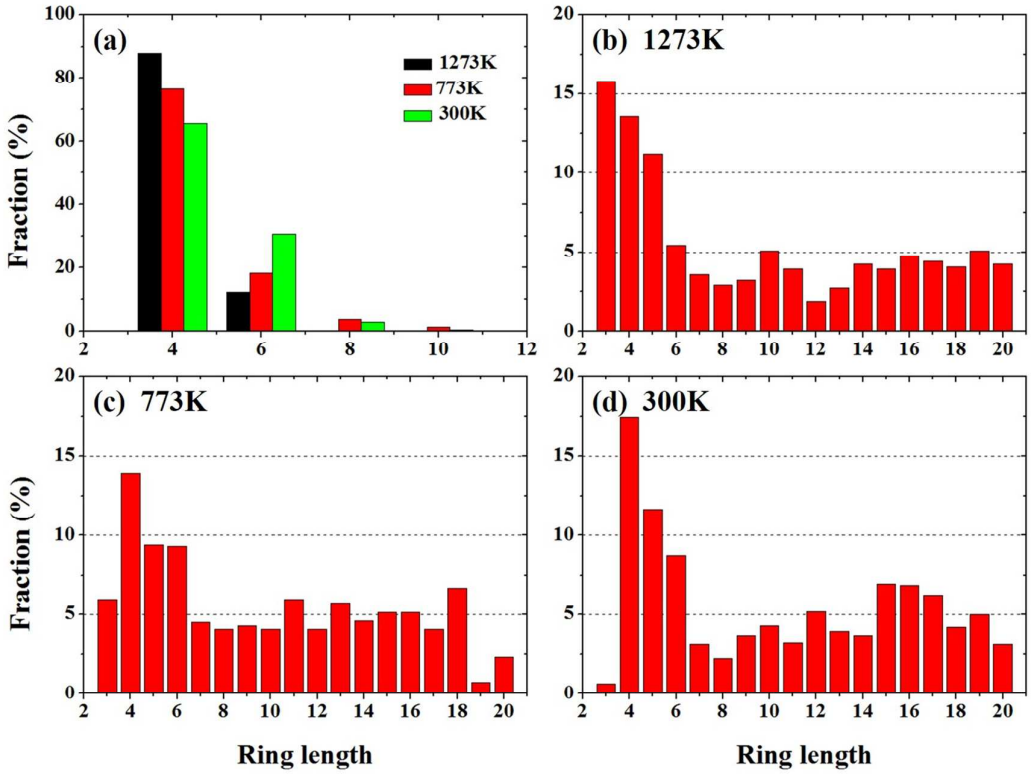

Figure 7. (a) Distributions of ABAB rings at different temperatures. Distributions of irreducible rings in GST at (b) 1273 K, (c) 773 K and (d) 300 K.

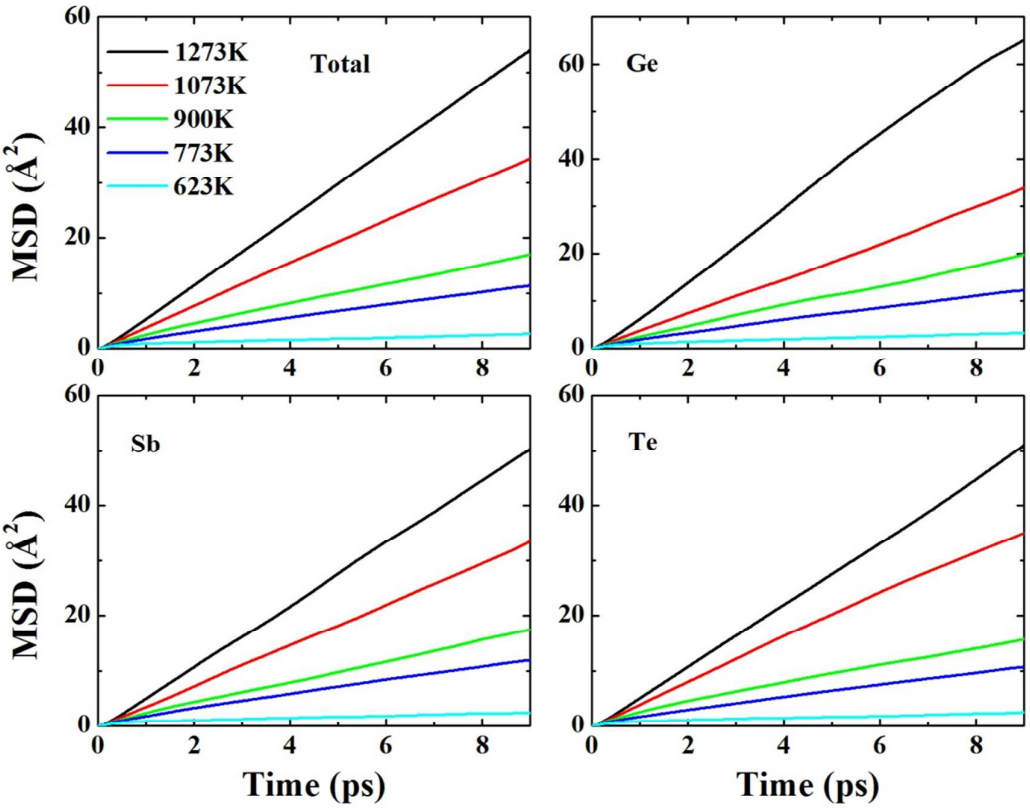

Figure 8. The MSD of GST at different temperatures.

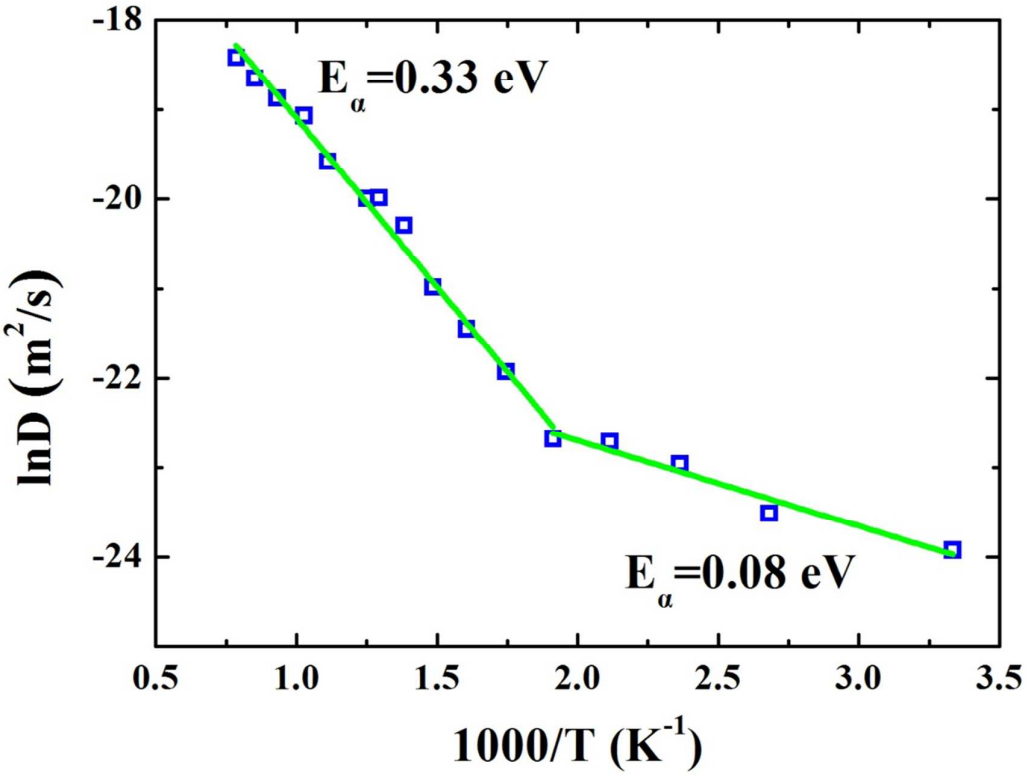

Figure 9. The diffusion coefficient D of GST at different temperatures

Graphical and textual abstract

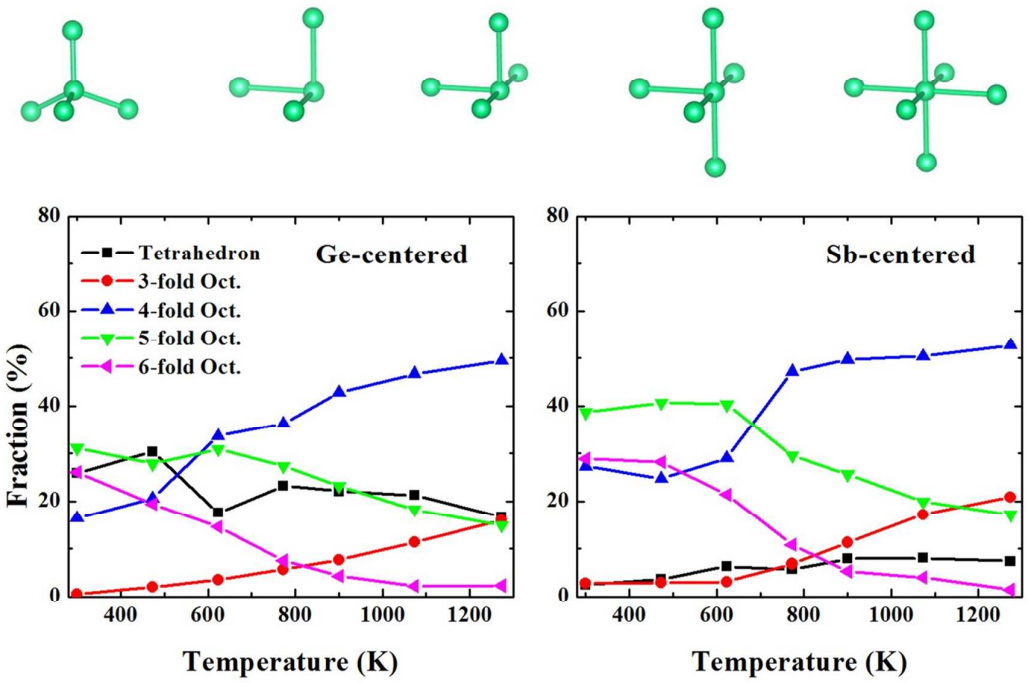

Five structures (tetrahedron and 3-, 4-, 5- and 6-fold octahedrons) are shown in the upper panels of the figure. Figures in the lower panels show the fractions of the five structures in Ge- and Sb-centered clusters with temperature.